Bulletin of the Geological Society of Finland, Vol. 93, 2021, pp 53–72 https://doi.org/10.17741/bgsf/93.1.004

Late Glacial and postglacial seismicity in the Northeastern Fennoscandian Shield: tectonic position and age of paleo-earthquakes near Murmansk

Svetlana B. Nikolaeva[1*], Mikhail V. Rodkin[2,3] and Sergey V. Shvarev[4,5]

[1]*Geological Institute of Kola Science Center RAS, Apatity, Russia*

[2]*International Institute of Earthquake Prediction Theory and Mathematical Geophysics RAS, Moscow, Russia*

[3]*Institute of Marine Geology and Geophysics, Far East Branch, RAS, Yuzhno-Sakhalinsk*

[4]*Institute of Geography RAS, Moscow, Russia*

[5]*Schmidt Institute of Physics of the Earth of RAS, Moscow, Russia*

VERTAISARVIOITU
KOLLEGIALT GRANSKAD
PEER-REVIEWED
www.tsv.fi/tunnus

Abstract

Earthquake-induced deformations located near Murmansk City were investigated for information on the age, tectonic position and spatial occurrence of paleo-earthquakes. The main earthquake-generating zone is identified to be the system of strike slip faults and reverse-oblique faults trending NNW along the Kola River valley. We used radiocarbon analysis and paleogeographic reconstructions and revealed three episodes of increased seismic activity: from 9500 to 10 500 cal BP, from 892 to 1182 cal BP, and from 200 to 300 cal BP. Based on the peak ground velocity estimation method we suggest that an earthquakes with a maximum moment magnitude up to Mw ≈ 6.0–6.5 may have taken place in the studied area. The recorded location of seismogenic deformation near faults indicates area of strong Late Glacial and Holocene earthquakes occurring in the northern Kola Peninsula; this is also consistent with observations concerning the historical events of 1772 and 1873, which took place near the area.

Combined with previous data on palaeoseismicity in Kola region, our studies indicate a longer lasting and more complex spatial and temporal history of postglacial seismicity in the Northeastern Fennoscandian Shield area. In contrast to the generally accepted opinion, strong seismic events occurred not only during the deglaciation period or immediately after it, but continued until the late Holocene and the last centuries. Glacial isostasy as a factor giving rise to stresses has become minimal by the present time, while the tectonic factor continues to be felt.

Keywords: earthquake-induced deformation, paleo-earthquakes, Fennoscandian shield, Kola Peninsula, Russia.

*Corresponding author (e-mail: nikolaeva@geoksc.apatity.ru)

Editorial handling: Antti Ojala (e-mail: antti.ojala@gtk.fi)

1. Introduction

The Kola region as the eastern periphery of the Fennoscandian Shield is characterized by rather low seismic activity at present. Yet, since 1542, several tens of both historical and instrumental earthquakes have been described and recorded in the region and adjacent territories (Mushketov & Orlov, 1893; Kondorskaya & Shebalin, 1982; Ahjos & Uski, 1992). A review of the literature suggests that the eastern (Russian) periphery of the Fennoscandian Shield from the Gulf of Finland to the Barents Sea has been subject to strong earthquakes over the past 10 000–12 000 years (Lukashov, 1995; Nikolaeva, 2001, 2008; Nikonov et al., 2014; Nikolaeva et al., 2018; Shvarev et al., 2018; Shvarev & Rodkin, 2018; Subetto et al., 2018). The late- and postglacial fragmentation of rocks, deformations in unconsolidated sediments also were the presumable cause of strong earthquakes (M_w ~ 7; I_0 = VIII–IX), as described by researchers for different localities in the western Fennoscandian crystalline Shield (Sweden, Norway, and Finland) (Kujansuu, 1964; Lagerbäck, 1992; Mörner, 2004, 2011; Olesen et al., 2004, 2013; Lagerbäck & Sundh, 2008; Kukkonen et al., 2010; Smith et al., 2014; Sutinen et al., 2018; Ojala et al., 2018; 2019).

It should be noted that the eastern, Russian, part of the Fennoscandian crystalline Shield differs from the most of Fennoscandia. It shows lower rates of postglacial uplift, hence lower uplift amplitudes (Yevzerov, 1988; Demidov et al., 2006). In the Kola region and Karelia, no long, continuous, postglacial fault scarps, such as in Norway and Sweden (extending for a few tens or hundreds of kilometers), have been detected on land. Crystalline rocks were more frequently found to contain individual ruptures and cracks (or their systems) that inherited older weakened zones (deep faults). Much more extensive data have been acquired on Late Glacial and Holocene earthquakes and their secondary effects.

Whilst instrumental records in seismology only cover decades up to a century, paleoseismology covers tens of thousands of years. The significance of the accumulation of additional reliable information on the spatial localization and age determinations of strong earthquakes of the past under these conditions increases.

These data are very important for assessing seismic risks in the Murmansk region, i.e., a territory with a well-developed infrastructure, mining enterprises, and nuclear power facilities. In the case of nuclear waste handling, the time span needed to be covered by seismic hazard assessment increases significantly (Mörner, 2011). Paleoseismology offers means of extending the record into the past and hence establishing an improved database for risk evaluations. However, the confirmation of the seismic origin and the determination of the paleo-earthquake parameters (magnitude and age) are poorly studied, and often cause discussions.

The present paper reports the results of the study of late- and postglacial deformation in bedrock and the unconsolidated deposits located near Murmansk City (northern Kola Peninsula) (Fig. 1). Numerous deformations in bedrock of presumably seismogenic genesis were first found in the 2000s (Nikolaeva, 2001, 2008). Since then, these structures have not been studied. In this article, we present new information on the age, tectonic position and spatial patterns of paleo-earthquakes in the studied area. We have used a radiocarbon analysis and paleogeographic reconstructions and identified three episodes of increased seismic activity in the Late Pleistocene and during the Holocene. Based on the peak ground velocity estimation method we have estimated the intensities of paleo-earthquakes (using the ESI-scale) (Michetti et al., 2007) and the possible pairs of values (magnitudes and the hypocenter distance) from our new approach based on evaluations of particle velocities that could cause the observed block displacements (Rodkin et al., 2012). Furthermore, combined with previous data on palaeoseismicity, we show that seismotectonic activity in the area continued not only in the late glacial time, but during the entire Holocene up to the last centuries.

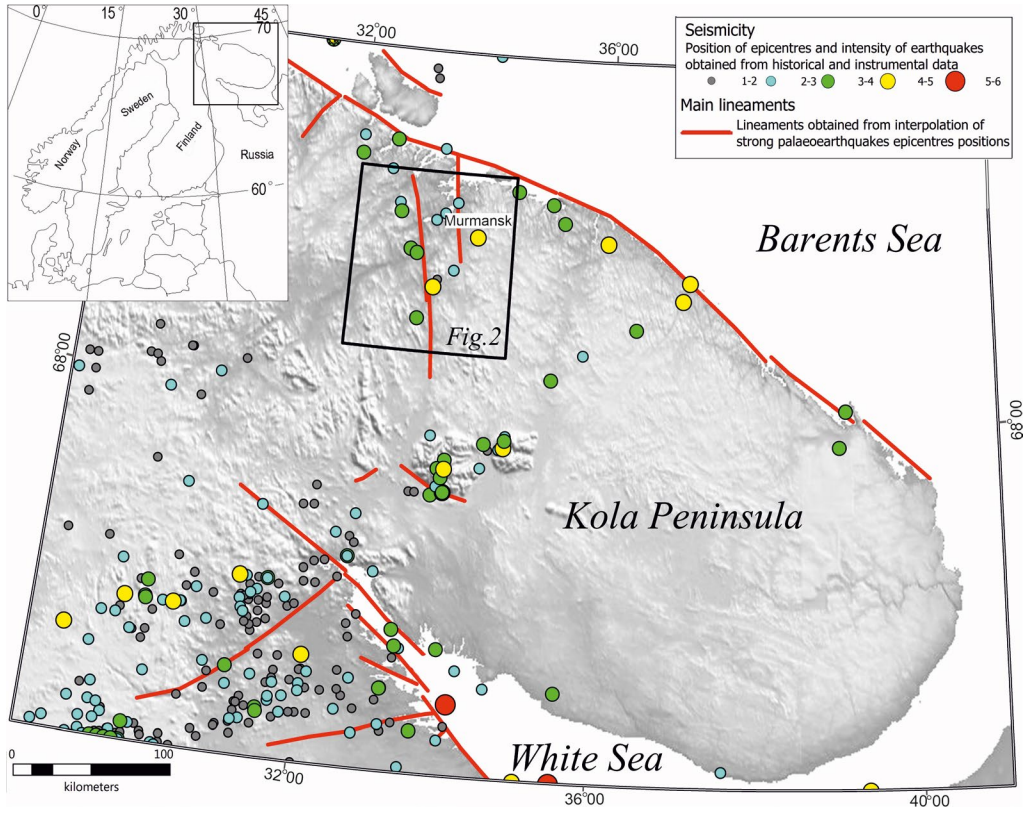

Figure 1. Location of seismic lineaments and earthquake epicenters in the northeastern part of the Fennoscandian crystalline shield. (Digital elevation model based on data GTOPO–30). The square shows the study area discussed in the article and the position of Fig. 2.

2. Methods

Assessment of the tectonic position and parameters of paleo-earthquakes is based on a methods used in two main stages of the study (McCalpin, 2009). At the first stage (identification of paleo-earthquake foci) we search for the seismogenic deformations and determine their structural position. At this stage, the following is distinguished: a) the neotectonic block structure of the territory as a potential framework of seismogenic faults; b) zones of concentration of disturbances in the topography as probable foci of postglacial earthquakes.

The selection of active faults, in the absence of significant modern seismicity in the studied area, is mainly carried out by morphological features. The faults, well-defined in the relief, under conditions of continuous spread of crystalline rocks, primarily reflect tectonically weakened zones, i.e., either directly tectonic landforms (grabens, normal and reverse fault scarps) or zones of fragmentation formed and processed by exogenous processes. Lithological differences that affect the selective denudation and morphological expression of linear structures are usually associated with tectonic contacts here, as well as fall into the category of potentially activated ones.

We used middle-resolution remote sensing data, i.e., Landsat-ETM+ satellite images (horizontal resolution of 30 m), as the basis for identifying the morphologically expressed newest block structure of the territory (http://glcf.umiacs.umd.edu), as well as digital terrain models of AsterGDEM (2020) and GTOPO30 (1996). The search of

postglacial terrain disturbances was carried out on the basis of analysis of high-resolution remote data: GeoEye and WorldView satellite images, archived aerial photographs from geodetic and geological collections (libraries) and high-resolution DEM (2 m) ArcticDEM (2020).

The detected areas of destruction of the postglacial rock surface (open cracks, gorges, ditches, scarps) serve as the basis for conducting detailed field studies and searching for seismogenic deformations in the unconsolidated late glacial and Holocene deposits. When analyzing potential seismic manifestations in the relief, basement rocks, and Quaternary sediments, they are critically analyzed in terms of correspondence to similar forms in active regions with known seismicity and criteria for active faults (Wheeler, 2002; Olesen, 2004; McCalpin, 2009; Owen & Moretti, 2011) and tested for a potential alternative origin of the studied objects (gravitational, sedimentary, glacial, cryogenic).

At the second stage (estimation of paleo-earthquake parameters), specific kinematic features of seismogenic structures, intensity, magnitude, and age of paleo-earthquakes, are studied. The identified seismogenic deformations are carefully studied in detail by establishing numerical parameters – length, width, depth, orientation of cracks and rock ledges, amplitude and direction of the vertical and lateral offsets along the faults, thickness of layers with liquefaction, and size of individual forms disrupting the normal layering of sediments.

To determine the age of events, we used a comparative stratigraphic method for determining the time of formation of breaks and liquefaction textures in terraced sediments in the Kola River valley (in relation to similar instrumentally dated sediments tested in the Murmansk area), paleogeographic reconstructions; and radiocarbon method. For radiocarbon dating, we used organic detritus buried in rockfall plumes. The samples were processed according to standard protocols in the certified Center for Collective Use "Laboratory of Radiocarbon Dating and Electron Microscopy" of the Institute of Geography RAS (Moscow) (Zazovskaya, 2016).

The identified quantitative parameters were compared to the ESI–2007 scale (Michetti et al., 2007) to determine the intensity of concussions at the site of deformities. An alternative estimate was made using a new method for estimating the earthquake magnitudes by movements of block fragments (Rodkin et al., 2012). We made use of the peak ground velocity estimation method (PGVEM) to estimate peak ground velocities (PGVs) from observed displacements of discrete bedrock bodies. The PGVEM method is based on the energy balance equation. This approach can be considered as an alternative to the numerical discrete element discontinuous deformation analysis (DDA) method (Kamai & Hatzor, 2008; Anderson, 2010) based on the use of the equation of motion. As it is common in mechanics the DDA method based of the equation of motion can be more exact, whereas the PGVEM based on the energy balance equation appears to be easier to use. By now, a considerable experience has been accumulated in the use of the PGVEM in the east of Fennoscandia (Nikolaeva et al., 2018; Shvarev & Rodkin, 2018; Shvarev et al., 2018; Rodkin & Korzhenkov, 2019).

3. Geological setting

The Kola region as an element of the northeastern Fennoscandian Shield is the largest representative of the Early Precambrian crystalline basement of the East-European craton. The region is composed of the ancient rocks of the crystalline shield, which crop out as a result of a long vertical uplift. The major Precambrian provinces of the Fennoscandian Shield are Lapland-Kola-Karelia, Svecofennian, and Sveco-Norwegian (Mitrofanov & Zozulya, 2002). Each province can be subdivided into units of a lower rank. According to geological and structural-tectonic studies, the study area is located in the Kola geoblock (domain, composite terrane) in the Central Kola structure. The major structure-forming elements of the area are NW-striking faults. Also, there is a NW-orientations of isoclinal imbricated structures. The area abounds in gneisses,

granite-gneisses, granodiorites, and enderbites, as well as intrusive rocks (Mitrofanov, 2001).

In the Kola region, the Late Weichselian ice sheet reached the maximum extent 16000–17000 years BP. The deglaciation was the fastest in the territory occupied by the Younger Dryas ice cover (Yevzerov, 1988; Stroeven et al., 2016). Glacioisostatic uplift of the region occurred due to deglaciation. This rise is dome-shaped; the western part of the Kola Peninsula rose more intensively than the eastern one. Such a tendency prevailed during the end of the Late Pleistocene and Holocene.

Quaternary deposits are mainly represented by Late Pleistocene sand-and-gravel moraines, fluvioglacial and glacial-lacustrine deposits, as well as eskers, deltas, and drumlins. Crystalline rocks of different types in areas with no continuous cover of glacial deposits are superposed by eluvium. Elongated eskers and drumlins strike in the SW-direction and coincide with the direction of the main ice lobes (Niemelä et al., 1993). Holocene deposits like peat bogs, lacustrine sediments, and lake bottom sediments occupy a much smaller area.

The entire history of geological and tectonic evolution in the region shows inherited movements in zones of larger older faults. The stress field, which was partly influenced by deglaciation, led to active failures in the bedrock, reactivation of pre-existing faults and caused earthquakes (Lagerbäck, 1992; Lukashov, 1995; Mörner, 2004, 2011; Olesen et al., 2004; Brandes et al., 2018).

Almost all of the modern earthquake epicenters were located at shallow crustal depths, ranging from 5 to 25 km, and are rarely deeper. Their magnitude (M_w) was 2–4 units and very rarely exceeded 4.6 (Ahjos & Uski, 1992). Historical earthquakes produced greater ground motion. Russian chronicles and newspaper publications recorded felt earthquakes in 1772 and 1873 in the northern Kola Peninsula (Mushketov & Orlov, 1893). The earthquake epicenters (N 68.7; E 33.3) with Mw = 4.6–5 and intensity I_0 = 6 were in the environs of the town of Kola (Kondorskaya & Shebalin, 1982) (Fig. 2).

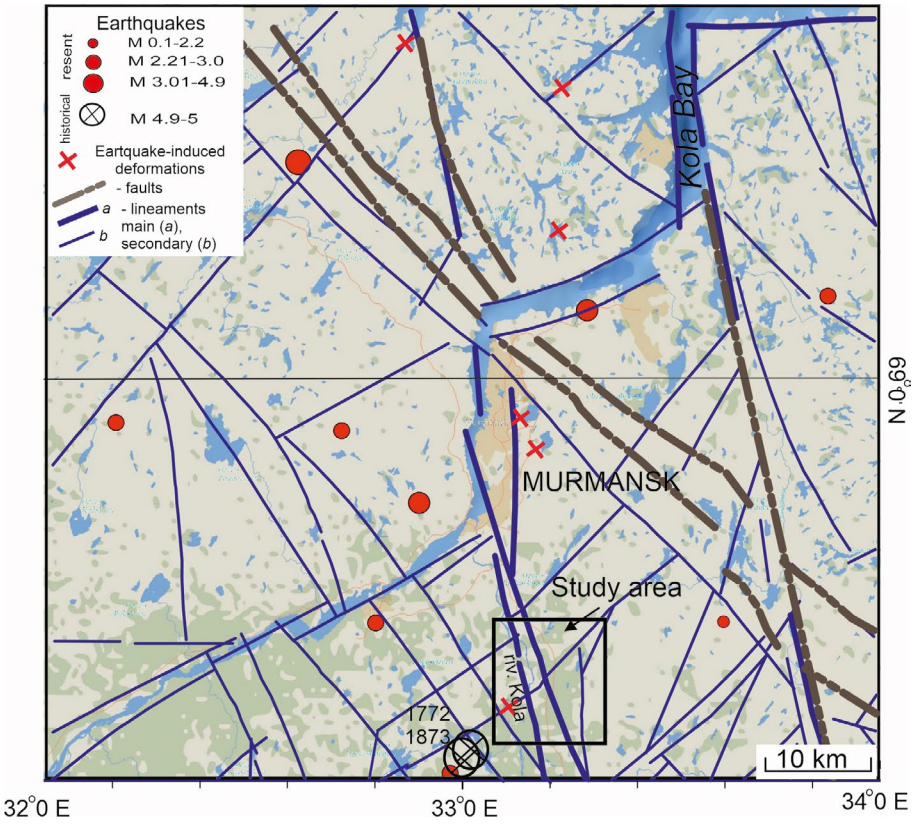

Figure 2. Map showing the earthquake epicenters for the period 1990–2009 (Ahjos & Uski, 1992), historical events of 1772 and 1873 (Mushketov & Orlov, 1893; Kondorskaya & Shebalin, 1982), seismically-induced deformations (Nikolaeva, 2008; 2013), main faults (Mitrofanov, 2001), lineaments identified in space images (Landsat–ETM+) and Digital Elevation Models (GTOPO–30, ArcticDEM) and the study area near Murmansk City (northern Kola Peninsula).

4. Results

The study area is located ca. 11 km south of Murmansk City on the eastern bank of the Kola River (Fig. 2). According to geomorphological data and interpretation of the satellite image (Landsat-ETM + and Digital Elevation Models), the proposed fault of NNW-trending follows the Kola River valley. The structure, whose segments extend along the Kola River valley is distinguished by morphological features (a series of separate faults arranged in an echelon pattern) and the occurrence of postglacial topography deformations and exogenous processes. The tectonic zone has a regional character and a total length of more than 100 km from the Kola Bay (in the north) to Lake Imandra (in the south). Along with a parallel fault located 20–25 km to the east with established right-shift displacements (Baluyev et al., 2012), it forms a single zone characterized by massive development of deformations in the relief, manifestations of exogenous processes, and modern weak seismicity (Kondorskaya & Shebalin, 1982). The site of intense deformation of rocks, as well as deformations in the unconsolidated deposits of the terrace of the Kola River, were found here on an area of ca. 5 000 km^2.

4.1. Earthquake-induced deformations in bedrock

We have analyzed in detail the bedrock deformation on the SW slopes of Mount Kildinskaya (Fig. 3a). The destruction zone is located near the western flank of the main NNW fault (345°–350°) near its intersection with the secondary NE (45°–55°) fault systems. The alternating narrow structural denudation bedrock ridges correspond to tectonic blocks, and lows related to fragmentation zones show that the relief has a tectonic origin in the studied area. The altitudes of ridge crests vary around 250–350 m a.s.l. reaching 400–450 m eastwards and northeastwards, while the intervening depressions are ca. 100–200 m lowering down to 70–90 m westwards and southwestwards. The top of bedrock has retained traces of glacial erosion and weathering everywhere. Upon the background of this "glacial relief", one can clearly discern the destruction area in bedrock. Intensive fragmentation of scarps and horst-shaped massifs, postglacial fissure systems, rockfalls, rockslides, collapses of big blocks, which are partly buried under the slope cover of colluvial deposits, and block displacements have been found in Precambrian gneisses and granite-gneisses.

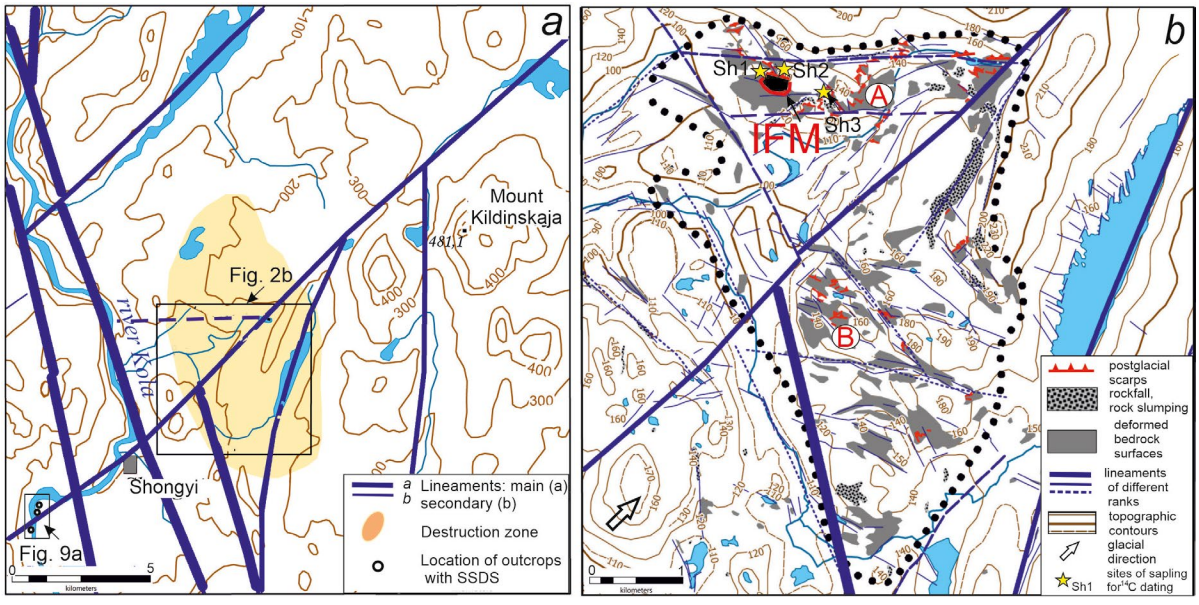

Figure. 3. Location of the study site: a) late- and postglacial deformation in bedrock and the unconsolidated deposits located near the Kola River valley, b) destruction zone studied in detail (explanation in the text).

The main feature of the destruction zone in the northern part (Fig. 3b, A) is isolated, large and intensively fractured horst-shaped massif (IFM) (Fig. 4). Such relief disturbances have not been previously described in the Kola region, so we will discuss this deformation in more detail.

IFM is a fragment of a fractured rocky sub-latitudinal ridge (125–130 m a.s.l.). The block is 300 × 300 m in size, composed of granite-gneisses, and bounded by scarps h=1.5–10 m on all sides (Figs. 4a-d). The colluvial apron zone is 0 to 20–30 m wide with large chaotically lying blocks and extends along the periphery of the massif. The several generations of slumped rock masses and traces of secondary displacements affecting individual large blocks occur in this zone. Basic and ultrabasic subvertical dikes with a thickness of 0.6 to 5.5 m intersect the granite-gneisses massif.

The massif is also intersected by open fractures; they are 15–20 cm to 85 cm wide (Fig. 5a). The orientation of the fractures has two main directions: 330°–350° and W–E (Fig. 4b). The edges of the massif show E–W splits and tension cracks >1–1.5 m wide and >5–8 m deep (throughout the entire thickness of the massif) that have removed vertical blocks as high as 6–8 m and 2–6 m in length from the scarps (Fig. 5b).

Fissures located within the rock massif are raised by 7–10 m above the surrounding relatively flat and horizontal surface. According to their "freshness", and the absence of glacial or glaciofluvial sediments inside the fissures, they formed after the last glacier melting. Their orientation demonstrate a systematic nature with 2 general directions. The maximum opening is observed in sublatitudinal cracks on the northern and southern flanks of the massif near its edges and associated with the extension of large blocks to the north and south. Thus, the following facts contradict the possible mechanism of "wedging" of water freezing in fissures or the jacking effect: 1) open hydrodynamic system: there are no conditions for water accumulation (after the

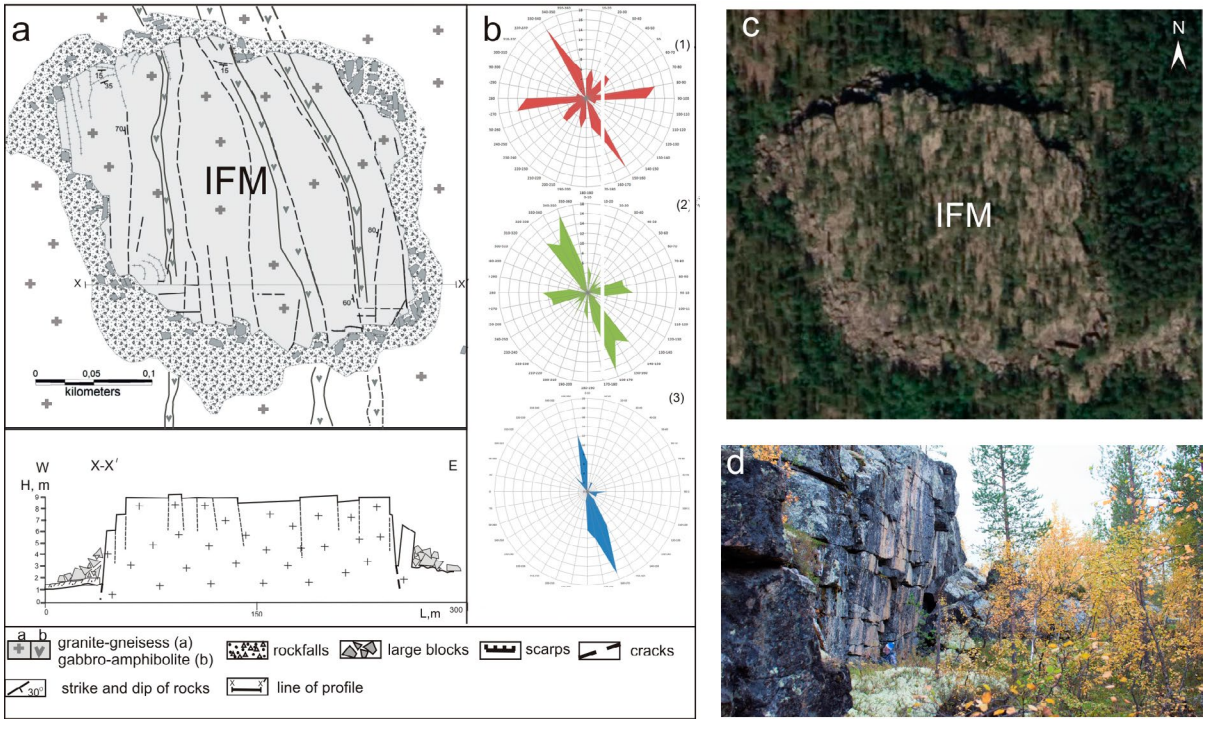

Figure 4. Intensively fragmented massif (IFM): a) plan and profile; b) rose diagrams: 1) orientations of fissures on the top of the massif, 2) orientation of fissures in marginal parts of scarps, 3) directions of movement of blocks dislodged from the massif; c) view of IFM from space (Google Earth Pro; Image U.S. Geological Survey); d) scarp that bounds the IFM to the north.

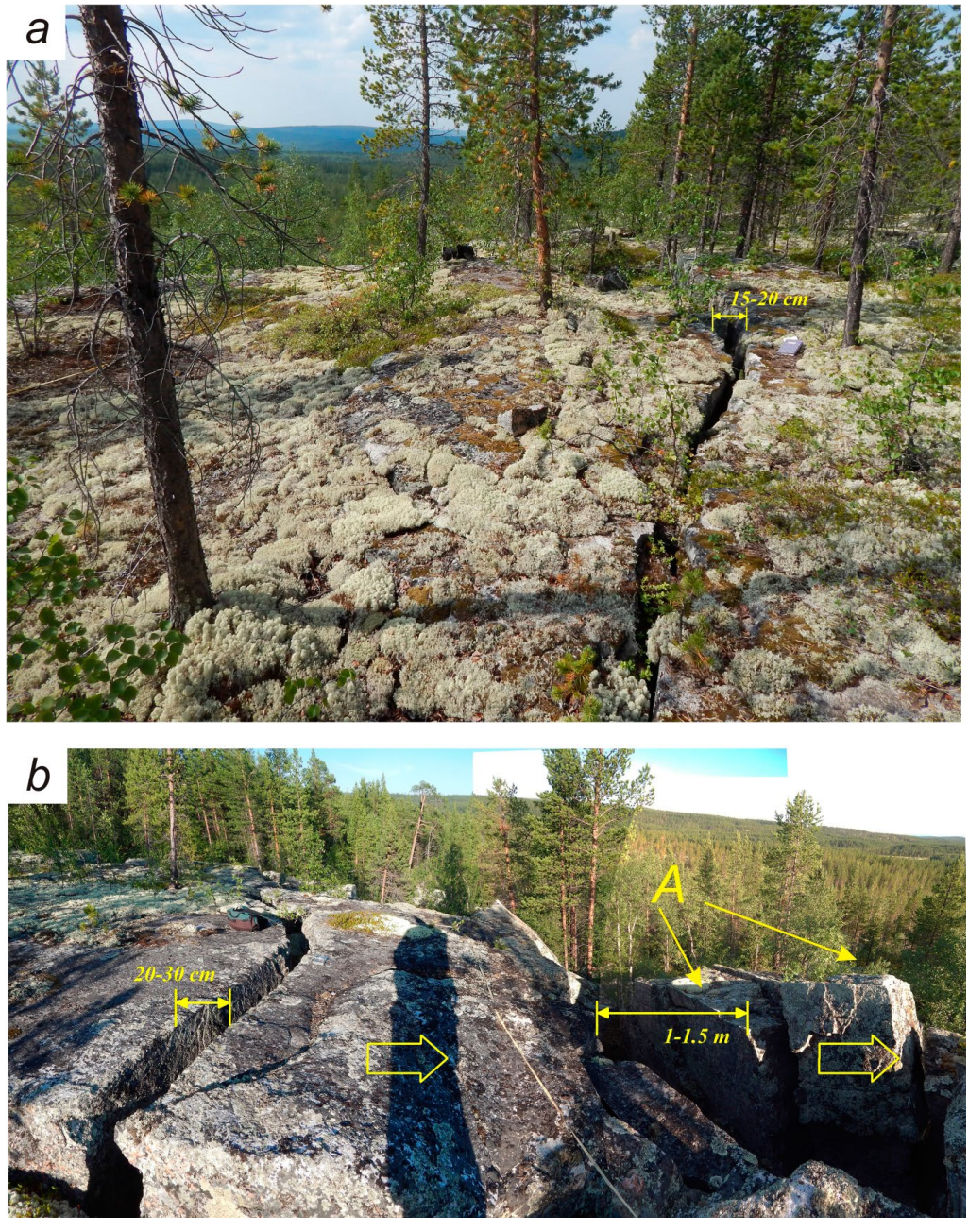

Figure 5.
a) Open fractures NNW–trending in granite-gneisses on the top of the massif,
b) E–W tension fractures and blocks (A) that have been moved southward (view from out the rim of the IFM).

deglaciation), 2) the systematic nature of fissures: subordination to the main directions; change in size in accordance with the structure; paragenetic series of cracks extending to the edge parts of the array, passing into gaping cavities separating completely detached blocks, which are replaced by collapse accumulations outside the massif, and 3) the fissures do not get narrow along the depth (downwards the massif), as would be expected in the case of wedging in the freezing and thawing processes (Lomtadze, 1977).

One of the subtypes of bedrock deformation is the displacement of individual crystalline blocks from scarps. We observe differences in the scale of block displacements and in the degree of rock crushing and analyzed such displaced blocks in

the scarps of IFM and at its periphery in zone A. The displaced blocks show three characteristic variants of position: 1) block toppling (stability solely controlled by discontinuity orientation and block shape); 2) flexural toppling (stability predisposed by discontinuity orientation and block shape, but fracturing through intact rock to form a basal release surface is required for failure); and 3) flexural-block toppling (an intermediate case where both bounding discontinuity and intact rock fractures are important to the failure) (Goodman & Bray, 1976). Toppling occurs when an unstable rock block rotates in a vertical plane about a fixed point. It is favored in columnar rock blocks on an inclined plane where the center of gravity of the block lies beyond its base. These variants are complicated by rotations about the vertical axis for blocks. In addition, we observed a displacement of a block with a volume of V ~ 80 m^3 in the lower part of the scarp (Fig. 6a), as well as a laterally displaced plate V ~ 0.005–0.007 m^3 (Fig. 6b) and other displacements of individual blocks (Figs. 6c, d & 7). These examples provide evidence of horizontal seismic pulses at work.

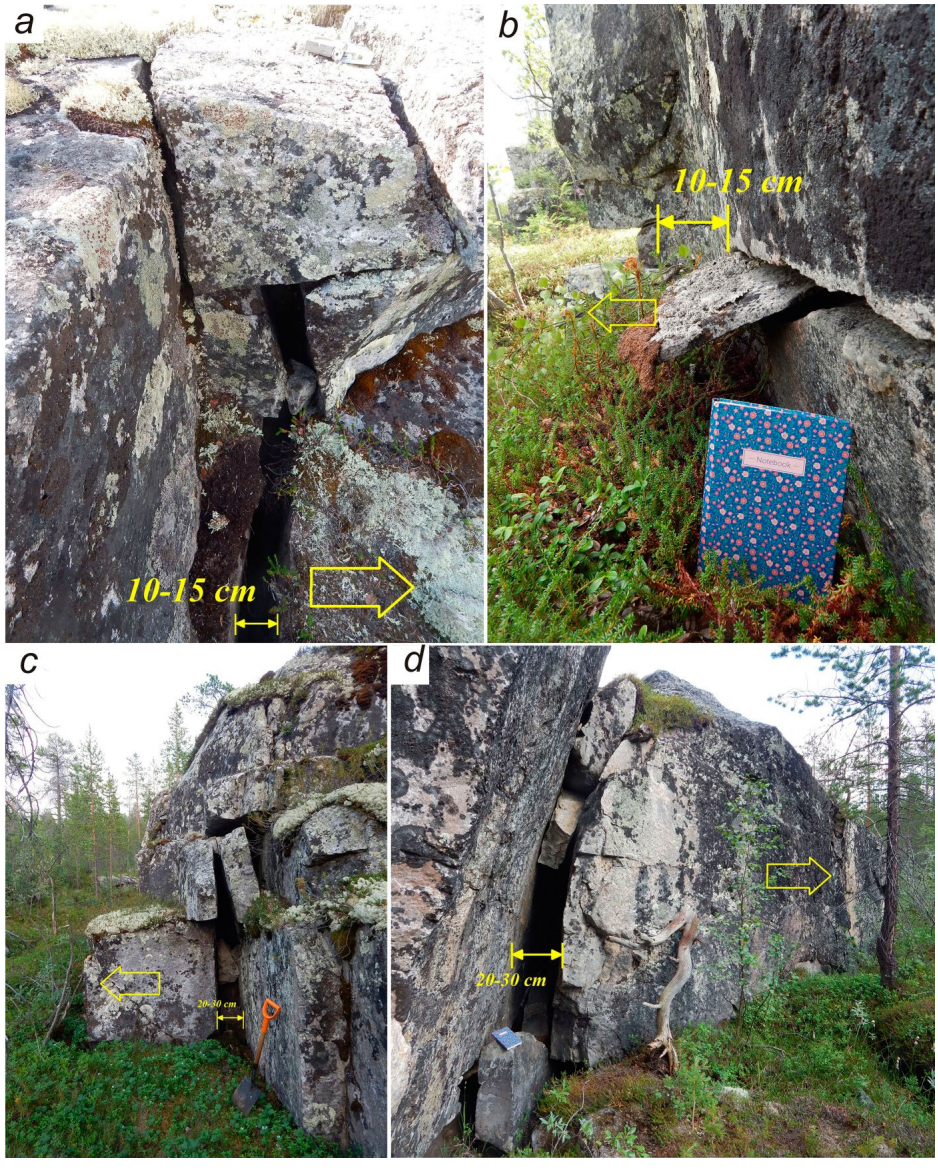

Figure 6. Displacement of crystalline blocks: a) the lower part of the IFM wall moved away (a block of about 80 m^3), b) 0,005–0.007 m^3 slab dislodged from a horizontal aperture at the IFM base, c) a block of about 1 m^3 dislodged from the base of a local massif, d) a 40–60 m^3 block pushed away from under the inclined wall of a local massif.

Fig. 7. A horizontal fissure in gneiss with the upper part pushed upwards.

The nearly horizontal surfaces adjacent to the IFM show split blocks that were displaced through distances of 3–8 cm from their original positions. Our study has revealed 152 cases of presumably earthquake-induced displacement and movement of bedrock blocks. A criterion to differentiate between the observed dislocation and a creep is the use of dislocations primarily located only along horizontal surfaces. At the same time, we additionally considered the slope, the direction of displacement of rock fragments. A creep may occur only downwards a slope. The block movements were horizontal with a minor vertical component, and with greater displacements at the lower depth levels, hence these deformations have no gravitational origin.

A diagram of the number of these displacements is shown in Figure 8a. The points, for which the displacement velocities V (PGV) have been obtained to determine the intensity and magnitude of earthquakes is shown in Figure 8b. The diagram in Figure 8a can be represented by a combination of three systems of oppositely directed displacement of local blocks (S1, S2, S3). We show, that the main trends in block displacements are NNW and W–E. At the same time, the maximum of displacements in the SSE and S direction is clearly distinguished, which indicates the passage of a seismic wave from north to south.

The morphostructure of IFM is controlled by cracks and ruptures of the NNW and E–W directions with a significantly lesser role of NE-

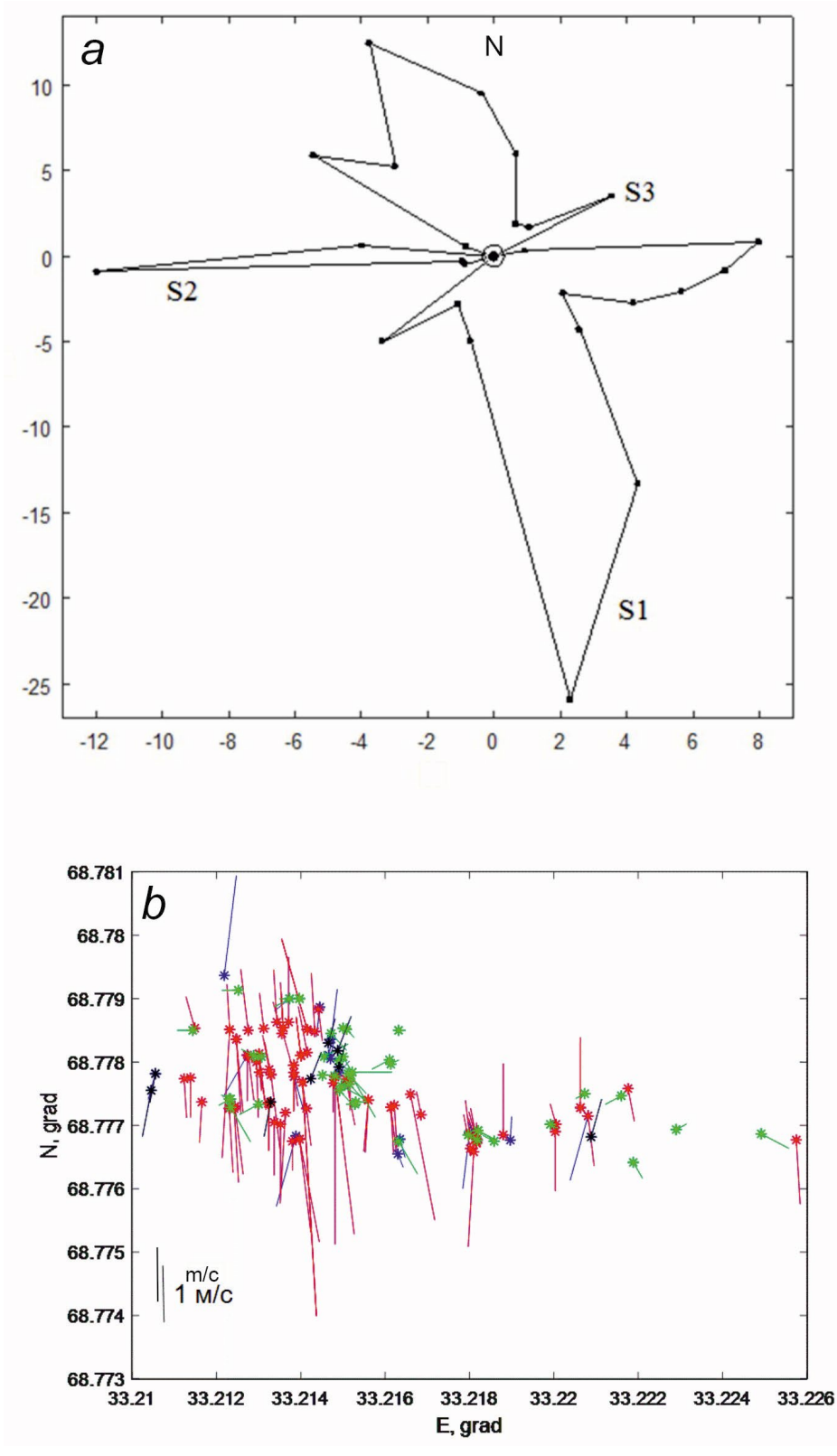

Figure 8. a) A rose diagram showing the direction of displacements, b) parameters of block movement in the IFM and environs. The arrow length on Fig. b corresponds to mass velocity, m/s; red arrows indicate displacements of the S1 system, green arrows show those of S2, and black arrows show S3 displacements. Blue arrows show a few displacements that do not fit either of the above systems. 1m/c – scale of block displacements.

trending. The same direction is the main one in the distribution of lateral displacements of block along the periphery of the massif.

The destruction zone in the southern part (zone B) contains sets of nearly parallel grabens or gorges and horst-shaped little ridges (extending along azimuth 300°–340°) with vertical scarps smoothed by glacial erosion (Fig. 3b, B). Along with them, the scarps show characteristic signs of postglacial activity: fresh slopes and broken glacial polish. Fault scarps contain recesses and protruding, partly dislodged blocks ("rock pillars" and "rock feathers").

Seismically induced deformation can also be seen in other local massifs where one finds long (reaching 50–100 m) vertical fissures of 10–20 cm wide. In some cases, the fracture edges were smoothened. In other cases, the fissures have sharp sides. Such differentiation can be explained by heterochronous generations of the fissures that formed both before the most recent glacial cover and after the glacier melted. The fissures have a clearly defined orientation (325°–340° and 30°–45°), the fault sides frequently show slickensides. The fissures have main kinematic types: reverse faults, strike slip, and their combinations.

According to Brideau & Roberts (2014) bedrock mass movements include some of the most common (rockfalls, rock slides, rock spread) and most destructive (rock avalanches) slope processes. The study area contains rockfalls and rock avalanches (Fig. 3b). The clastic material in the rockfalls includes both angular (jagged, unrounded) blocks and well-rounded boulders, thus indicates multiple resumptions of seismic activity in that zone and the "preparation" of the blocks due to preglacial seismic events. The subsequent glacial action aligned the blocks, while the postglacial seismic events produced a partial fragmentation.

4.2. Soft-sediment deformation structures (SSDS)

4 km to the southwest of the destruction zone on the scarp of the terrace (h = 10 m) of the Kola River, soft-sediment deformation structures (SSDS) were found (Fig. 3a). The terrace is composed of sands and gravel-pebble sediments of river alluvium (Unit 1), glaciolacustrine rhythmically stratified fine sands and sandy loams (Unit 2), glacial marine clays (Unit 3) (Fig. 9a). In the Unit 2, SSDS occur mainly separated by undisturbed layers, are sandwich-shaped, and are extended laterally to some hundreds of meters. SSDS show two types of deformation: brittle and plicative.

The brittle type of deformations is dominated by a combination of shear deformation bands and shear-reverse faults, whose amplitudes of displacement are 3 to 20 cm, and dikes with a thickness of 3–4 mm to 1–1.5 cm. The dikes are filled with light-colored homogeneous sand supplied from lower horizons (Fig. 9b, c). These deformations could not have been produced by slope gravity, because the cracks dip into the slope or diagonally to the natural slope of the terrace. We also exclude the possibility that these deformations bands are caused by high pore pressures under glacier. As it will be shown in section 4.3, the deposits were formed in warm conditions, in periglacial lake basins, when there was no thick ice. A clear sign of seismic origin is a combination of brittle and plastic deformations in one layer (Obermeier et al., 2005; Owen & Moretti, 2011; Lunina et al., 2012).

The sets of deformations bands could have been formed in the overlying layers by the passage of seismic waves (shear and tension fissures). Open cavities in fissures are channels to force out and eject liquefied material at times of anomalous increases in pore pressure, as well as to drag particles from the underlying layers during fluidization.

Fracture sand dikes in the sand are generally oriented along a consistent trend. Most of the fractures dip to the southeast (mean dip direction: 145°–160°) with mean inclination angles of ca. 55°–60°. Examination of rupturing deformation features suggests a hypothesis that they are associated with the activation of the NE-trending fault (Fig. 3).

The plicative deformations include bends and turnings of layers, which produce various folds and traces of liquefaction and fluidization

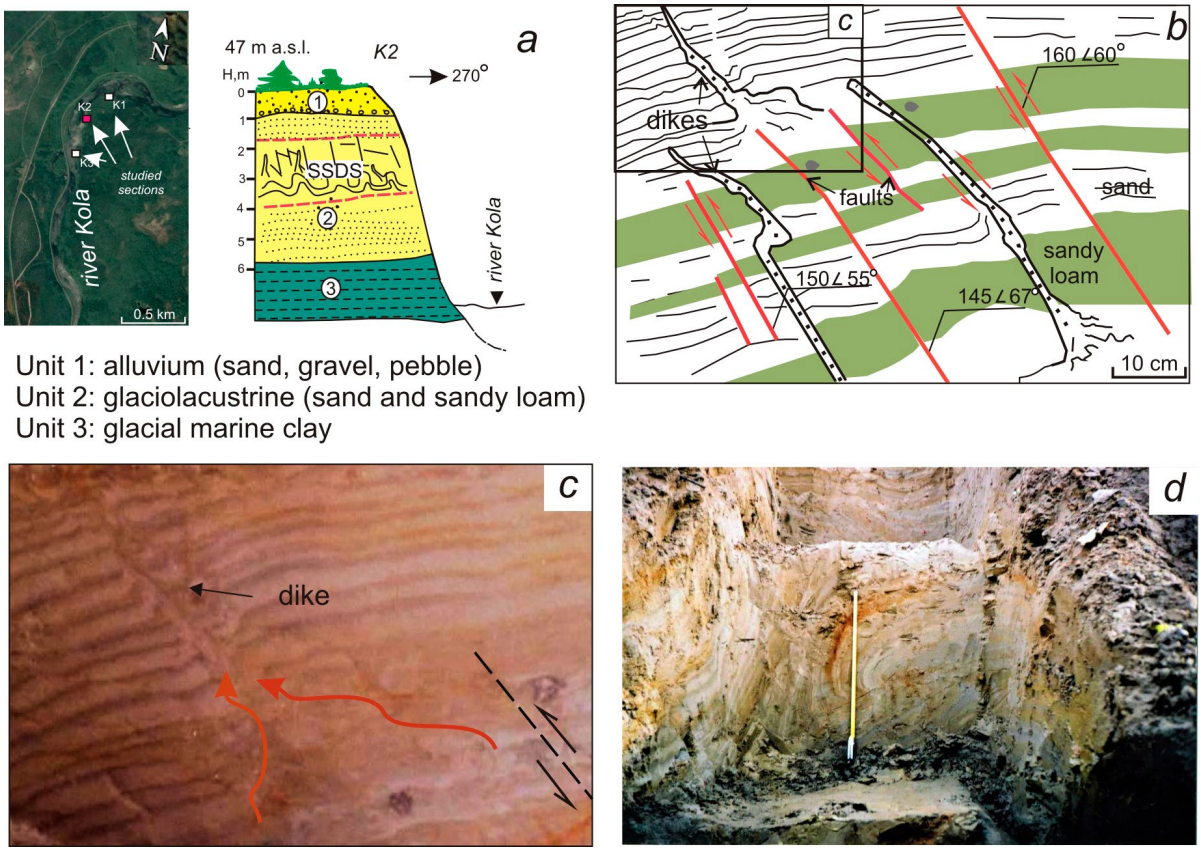

Figure 9. Soft-sediment deformation structures in Late Pleistocene sediments of the Kola River terrace: a) location of outcrops with deformations and section K2, b) – combination of shear deformation bands and shear-reverse faults, c) – sand dike (a fragment of fig b, photo), d) folds, flexures, and liquefaction occurrences.

(Fig. 9d). They were formed in liquefied layers or unconsolidated strata due to mixing of sediment, lateral overflow, and submergence or rise of layers with different physical and mechanical properties. The deformations occurred due to seismically-triggered slumping. These SSDS could have been formed by two different events or by an aftershock following the main event.

4.3. Ages of paleo-earthquakes

Radiocarbon analyses, the relationships between relief forms, and paleogeographic reconstructions, all of them point to the hypothesis that the deformations in rocks and unconsolidated sediments occurred due to several discrete events. The morphologic features of the deformations clearly divide them into two main sets, those, which occurred before, and those after the last glaciation, which can be inferred from the combinations of cracks in the massifs on the one hand and of clastic material with traces of glacial reworking or without it on the other. The several generations of slumped rock masses and traces of secondary displacements affecting individual large blocks provide evidence of multiple relief rejuvenation during the late glacial and postglacial periods. We have identified three events with a varying reliability degree.

In the set of traces of earthquakes caused by the *event I,* we include the following observation: fragmentation of bedrock massifs resulting in the formation of fissures that are occasionally as long as 100 m, the separation of marginal blocks from the IFM, the generation of rockfalls and stone-and-

Table 1. Radiocarbon ages and mean calibrated years (2σ, 95.4% probability) of the organic matter buried by the rockfall. Calibration is based on IntCal13 and MARINE13 (Reimer et al., 2013).

Sample ID	Coordinates	Depth, cm	Material dated	^{14}C age, (yr BP)	Mean cal yr BP (2σ, 95.4%)	Lab ID
Sh1	N 68°46'42.99'' E 33°12'46.34''	50	paleosoil	1080±80	892–1182	6883 IGAN
Sh2	N 68°46'42.86'' E 33°12'51.00''	20	mixture of peat and soil	210±60	58–325	6882 IGAN
Sh3	N 68°46'37.78'' E 33°13'14.19''	25	mixture of peat and loam	260±60	258–490	6884 IGAN

block avalanches, and lateral displacements of large (occasionally as large as 50–80 m^3) blocks.

We relate the *event I* to the generation of SSDS in the unconsolidated deposits of the Kola River valley. The fine sands, sandy loams, and the rhythmic stratification indicate sedimentation in the near-glacier basin that had existed during late glacial period at the last phases of the deglaciation (Yevzerov & Nikolaeva, 2007). The spore-pollen spectra of the sections studied here reflect a gradual amelioration of the climatic conditions from arctic and subarctic periglacial to subarctic boreal conditions (Nikonov, 1964). The deposits were formed in periglacial lacustrine basins during the period from the Younger Dryas to the Pre-Boreal, ca. 11 000–9500 calibrated years BP (cal BP). Similar age estimates also apply to an earthquake-induced landslide of a moraine near Murmansk City, namely, 8950±150^{14}C yr BP (10 516–10 216 cal BP) (Yevzerov & Nikolaeva, 2007). Thus, the time of this earthquake *I* appears to be between 10 500–9500 cal BP.

In the set of co-seismic deformation due to the Late Holocene events (*events II* and *III*), we have included multiple rock fragmentation and the opening of existing cracks, the generation of secondary clastic colluvial around a bedrock outlier, local displacements of blocks, and dislodging individual blocks off scarp walls. To determine the age of the events, we have taken samples of organic material buried under rockfalls and rockslides (Fig. 3b). Samples were extracted under large landslide blocks exceeding 3 m in diameter, tightly lying on unconsolidated sediments without gaping cavities. The blocks are submerged by 20–30 cm in relation to the modern surface. The material for dating was extracted under the blocks with a lateral distance of up to 20–30 cm from the edge. This ensures a reliable burial of organic sediment *in-situ*, exclusion of post-collapse development of the vegetation cover under a colluvial block, or introduction of organic material.

The age of the *event II* correlates with the time when a small slump earth flow with a thickness of 0.5–0.7 m was formed; it is overlain by a rockfall near the northern wall of the IFM. The sample Sh1 was dated as 1182–892 cal BP (Table 1).

Event III is the youngest of the three. Two samples Sh2 and Sh3 of mixed peat and soil beneath rockfalls taken in the near and far peripheries of the IFM have showed similar ages (Table 1). These dates correspond to the upper age limit for the formation of the piles of blocks, their last generation. Thus, *event III* took place 200–300 years ago. Around the same time, the historical earthquake of 1772 was recorded, the epicenter of which was near the village of Kola (Mushketov & Orlov, 1893; Kondorskaya & Shebalin, 1982) (Fig. 1).

4.4. Intensities and magnitudes of paleo-earthquakes

Intensity (I_0) and possible magnitude (M_w) of ancient earthquakes have been determined using the ESI-2007 intensity scale (Michetti et al., 2007; Aptikaev, 2012), as well as the PGVEM method (Rodkin et al., 2012). The PGVEM makes uses of an equation that expresses the balance of

mechanical energy to find the original velocity V that have been imparted to a given piece of rock (rock fragment) to move it to a new position. The overwhelming majority of such cases can be treated using the simplest model for the displacement of a rock fragment through a distance L along a nearly horizontal surface with friction where the velocity V is estimated as

$$V = \sqrt{(2g \times k \times L)}, \qquad (1)$$

where *g* is the gravity acceleration and *k* is the frictional constant (k = 0.7). The velocity V we will identify with peak ground velocity, PGV.

Applying the PGVEM method to the analysis of block displacements in the epicentral zones of recent large earthquakes, we have found that the displacements usually occur in one (or two) oppositely directed azimuths. It is known that a train of waves from an earthquake usually contains one greatest amplitude that essentially exceeds the amplitudes of other vibrations. We assume that this high amplitude is related to the maximum mass velocity (PGV) that makes the rock blocks move into new positions (Rodkin & Korzhenkov, 2019). We expect the similar regularity in paleo-earthquakes.

Measurements and estimates of the directions and particle velocities V for different specimens are shown in Figures 8a and 8b. According to our analysis, the displacements of the S1, S2, S3 systems are rather uniformly distributed around the IFM (Fig. 8a). They are also uniform with respect to the sizes of the displaced bedrock blocks. Here with, the displacement vectors in the north mostly directed northwards, while those in the south systematically directed southwards. The similar pattern has been observed earlier near the rupture zone of the Kemin earthquake, northern Tien Shan (1911, Ms = 8.2) that went across the studied area (Rodkin & Korzhenkov, 2019).

Figure 8 gives a rather complex pattern of presumably earthquake-induced deformations, which provides a definite ground to suggest the occurrence of several strong paleo-earthquakes at the site. According to the existing intensity scales, *event I* had an intensity $I_0 \geq$ IX (Michetti et al., 2007). Similar estimates result also from using regression relations between intensity and the values of PGV, as estimated above (Aptikaev, 2012); between intensity and the PGV values; hence assuming PGV = 1.0–1.5 m/s, we have $I_0 = 9.5 \pm 0.8$.

The estimates of magnitude and the distance to the earthquake epicenter are more uncertain. After McGarr & Fletcher (2007) and Aptikaev (2012), the maximum value of PGV (namely, a few meters per second, possibly as great as 5–6 m/s) is independent of earthquake magnitude and depend on the rock rigidity and the type of fault movement (thrust fault, normal fault, or strike-slip fault). Magnitude of earthquake determines the distance to the fault where these maximum PGV values are possible.

Alternatively, after Douglas (2002), a scaled growth in PGV concurrently with increasing magnitude as d lg (PGV) / d Mw = 0.375 could be expected. The first of these inferences seems to agree with the strong motion better; hence if the distance to the nearest fault along the Kola River or historical earthquakes is ca. 2.5 km, the minimum possible magnitude of the responsible earthquake will be M_w = 6.0–6.5. In the case, if the seismic fault transected the IFM site, the earthquake magnitude could be less. After Michetti et al. (2007), the formation of secondary seismic-gravity rockfalls and the opening of existing fissures (*event I* and *event II*) would require the intensity I_0 = VII–VIII and M_w~6.

5. Discussion

One of the main tasks of the investigations was to establish that the formations attributed to the deformations (block displacements, fissures, rock-falls, rock slumping, and intensive fragmentation of scarps) are really of seismogenic origin. Since other processes also can reactivate faults or generate elements that can imitate a seismogenic deformation, those processes must be meticulously

excluded. The study area was repeatedly covered by ice sheets (Stroeven et al., 2016). Thus, it was important to demonstrate that the features investigated were not caused by glacial processes (differential erosion or ice-plucking, collapse due to melting of buried ice, glaciotectonics) or intensive physical weathering of crystalline rocks.

Deglaciation of the Kola Peninsula finished in the early Holocene ca. 11 500–9500 cal BP (Yevzerov, 1988). Unconsolidated sediments are relatively thin (6–10 m), but also fill in significant depressions in preglacial relief. Outcrops of bedrocks with a relative height of 5–10 m were exposed to active glacial erosion. All earlier weathering products and older sediments deposited, and fragments of rocks in gravitationally unstable sites were transported to lower hypsometric levels. Therefore, in areas where glacial formations occur, positive topographical features of the preglacial landscape consisting of massive new rocks were exposed. Since such areas were not subsequently weathered or covered by postglacial sediments, they were more vulnerable to seismogravitational rockfalls and landslides. Near the base of scarps dislodged blocks provide evidence of horizontal shocks and high frequency fluctuations. So, we conclude that these deformations are not associated with glacial erosion.

The fissures observed in the bedrock mainly differ from the fissures formed by frost weathering as follows: 1) The fissures have a specific definite orientation, while the frost fissures are characterized by random orientation; 2) The fissures do not get narrower along the depth (downwards the massif), as would be expected in the case of wedging in the freezing and thawing processes (Lomtadze, 1977); 3) On the fracture wings (in the fault plane), slickensides, tectonic indicators, can be often observed. Based on the absence of glacial or fluvioglacial sediments inside the fissures, part of they formed after the melting of the last glacier.

The argument in favor of the seismogenic nature of the rock fragment displacements is their orientation and statistics. As we showed in section 4, the block displacements have several dominant displacement directions, especially with a prevalence of displacements of opposite directions. Such oppositely directed displacements are very expected in the case of seismic action, but they appear to be unlikely in the case of the ice load.

The main criteria for the potential seismogenic genesis of deformations in unconsolidated sediments of the Kola River valley are as follows (Wheeler et al., 2002; Owen & Moretti, 2011): 1) their occurrence close to the major fault; 2) their presence in several outcrops in the same stratigraphic interval; 3) their large lateral extent, although high lateral variabilities of the deformation style, pattern, and bed thicknesses are possible, depending on the susceptibility of the sediments for liquefaction and/or fluidization, and 4) close location of late- and postglacial dislocations in bedrock. It should be noted that the combination of dikes and fractures in thin-stratified rhythmic sediment is similar to *fault-graded beds*, i.e., the type of textures described in the work of A. Seilacher, it almost always reflects earthquake-related genesis of deformation (Seilacher, 1969). Fluidization and liquefaction, as well as the above-mentioned combination of brittle and plicative deformations in the same section as observed in sections in the Kola River valley, unequivocally indicate a seismogenic genesis and a possible relation to different events or aftershocks. In addition, the set of fissures and dikes are generally oriented along a consistent trend, which suggests a hypothesis that they are associated with the activation of the NE-trending fault. After Brandes & Tanner (2012), these deformations bands are good indicators for fault activity.

Historical and recent seismicity is another important evidence. The epicenters of the 1772 and 1873 earthquakes (M_w=4.6–5 and I_0~6) are in the immediate vicinity of the study area where rock failures were identified (Fig. 1). These facts indicate the inherited nature of the instrumentally recorded earthquakes and a relative stability in their epicenter areas. According to the classical law of seismicity (the Gutenberg-Richter recurrence law), the probabilities of strong and weak earthquakes are clearly related (Gutenberg & Richter, 1944).

The main seismogenic zone is identified to be the system of strike-slip and oblique-slip faults stretching to the NNW along the Kola River valley. The kinematics of the zone are determined by the presence of reverse faults in unconsolidated sediments and directed systematic displacements of blocks along the strike of the fault zone.

Evidence of strong earthquakes during the late and postglacial periods were also described in Russian Karelia (Lukashov, 1995; Nikonov & Zykov, 1996; Shvarev & Rodkin, 2018; Shvarev et al., 2018) and other areas of the Kola region (Avenarius, 1989; Nikolaeva, 2006, 2009, 2013; Verzilin et al., 2013; Marakhanov & Romanenko, 2014; Nikolaeva et al., 2018). For example, the age of three seismic events (including the late glacial ones) was established in the area of the Lake Imandra depression in the Kola region centre (Nikolaeva et al., 2018). Three heterochronous pulses (~13 500, 10 300–7100, and 2500 cal BP) of strong seismic impacts were established in the study area. In the Kandalaksha graben of the White Sea, several generations of disturbances in crystalline rocks were found during the Holocene. The age of the youngest generation of seismic dislocations is 1900–1800 cal BP (Marakhanov & Romanenko, 2014).

The formation of co-seismic deformations and the activation of faults (or their segments) in the Late Holocene (the last 2000–3000 years) could no longer be dependent on the glacioisostatic effect. The spatial extent, locations, and orientations of the late glacial and postglacial faults and large earthquakes in this large region, as well as their distribution over time after the deglaciation, provide probable stems from the decaying glacial isostatic rise of the shield and from the passage from vertical glacial isostatic forces to horizontal compression.

6. Conclusions

1. The wide variety of studied local deformations, concentrated in a limited area near Murmansk in the northern Kola Peninsula, indicates an epicentral area of strong paleo-earthquakes. The main earthquake-generating zone is identified to be the system of strike slip faults and reverse-oblique faults NNW-trending along the Kola River valley. This main zone was intersected by northeast and local east-west striking faults, whose activity extended well into the Holocene. Deformations in the massif can be interpreted as connected with the seismic impulses oriented in S and SE directions.
2. Radiocarbon age data and paleogeographic reconstructions revealed three episodes of increased seismic activity from 10 500 to 9 500 cal BP, from 1182 to 892 cal BP, and from 300 to 200 cal BP. Based on the peak ground velocity estimation method we suggest that an earthquake with a maximum moment magnitude of up to Mw ≈ 6.0–6.5 may have taken place in the studied area. These estimates are in good agreement with the preliminary calculated magnitude estimates from other regions of Fennoscandia (Russian Karelia, Finland, and Sweden) (Mörner, 2004, 2011; Shvarev et al., 2018; Ojala et al., 2019).
3. The area where the earthquake-induced deformations in bedrock are concentrated is near the epicenters of the historical earthquakes of 1772 and 1873, thus indicating an inherited character of the instrumentally recorded earthquakes and a relative stability in their epicenter areas.

Combined with previous data on paleoseismicity in Kola region, our studies indicate a longer lasting and more complex spatial and temporal history of postglacial seismicity in the Northeastern Fennoscandian Shield area. In contrast to the generally accepted opinion, strong seismic events occurred not only during the deglaciation period

or immediately after it, but continued until the late Holocene and the last centuries. Glacial isostasy as a factor giving rise to stresses has become minimal by the present time, while the tectonic factor continues to be felt.

Acknowledgements

The research was carried out under research topics of the Geological Institute of the Kola Science Center RAS (Apatity) (project 0226-2019-0054), Institute of Physics of the Earth RAS (Moscow) (project 0144-2014-00097), Institute of Earthquake Prediction Theory and Mathematical Geophysics (topic AAAA-A19-119011490129-0), and of the Institute of Marine Geology and Geophysics, Far East Branch, Russian Academy of Sciences (topic AAAA-A18-118012290125-2.2). We thank A.O. Koroleva for taking part in field work. Finally, we are greatly indebted to two reviewers, Dr. Jussi Mattila and anonymous reviewer, who put time-consuming and tedious effort into raising the standards of the manuscript.

References

Ahjos, T., & Uski, M., 1992. Earthquakes in Northern Europe in 1375–1989. Tectonophysics 207, 1–23. https://doi.org/10.1016/0040-1951(92)90469-M

Anderson, J. G., 2010. Source and site characteristics of earthquakes that have caused exceptional ground accelerations and velocities. Bulletin of the Seismological Society of America 100, 1–36. https://doi.org/10.1785/0120080375.

Aptikaev, F. F., 2012. Instrumental Scale of Seismic Intensity. Moscow: Science and Education, 175 p. (In Russian).

ArcticDEM, 2020. Index of/elev/dem/setsm/ArcticDEM/mosaic/v3.0. http://data.pgc.umn.edu/elev/dem/setsm/ArcticDEM/mosaic/v3.0/

AsterGDEM, 2020. ASTER Global Digital Elevation Model. https://gdemdl.aster.jspacesystems.or.jp/index_en.html

Avenarius, I. G., 1989. Morphostructural analysis of the zone of neotectonic dislocations on the southern slope of the Kbibiny Mountains. Geomorfologiya 2, 52–56. (In Russian).

Baluyev, A. S., Zhuravlev, V. A., Terekhov, E. N., & Prahiyalgovsky, E. S., 2012. Tectonics of the White Sea and Adjacent Areas. Explanation to the Tectonic Map of the White Sea and Adjacent Areas 1:1 500 000, GEOS: Moscow, 104 p. (In Russian).

Brandes, C., & Tanner, D. C., 2012. Three-dimensional geometry and fabric of shear deformation bands in unconsolidated Pleistocene sediments. Tectonophysic 518, 84–92. https://doi.org/10.1016/j.tecto.2011.11.012.

Brandes, C., Steffen, H., Sandersen, P. E., Wu, P., & Winsemann, J., 2018. Glacially induced faulting along the NW segment of the Sorgenfrei-Tornquist Zone, northern Denmark: Implications for neotectonics and Lateglacial fault-bound basin formation. Quaternary Science Reviews 189, 149–168. https://doi.org/10.1016/j.quascirev.2018.03.036.

Brideau, M.-A. & Roberts, N. J., 2014. Mass movement in bedrock. Landslide Hazards, Risks and Disasters, 43–90. http://dx.doi.org/10.1016/B978-0-12-396452-6.00003-3

Demidov, I. N., Houmark-Nielsen, M., Kjær, K. H. & Larsen, E., 2006. The last Scandinavian ice sheet in northwestern Russia: ice flow patterns and decay dynamics. Boreas 35, 425–443. https://doi.org/10.1080/03009480600781883

Douglas, J., 2002. Note on scaling of peak ground acceleration and peak ground velocity with magnitude. Geophysical Journal International 148, 336–339. https://doi.org/10.1046/j.1365-246X.2002.01585.x

Goodman, R. E. & Bray, J. W., 1976. Toppling of rock slopes. In: Specialty Conference on Rock Engineering for Foundations and Slopes. American Society of Civil Engineering, Boulder, United States, 201–234. https://doi.org/10.4236/ijg.2017.83014

GTOPO30, 1996. Global 30 Arc-Second Elevation (GTOPO30). DOI: /10.5066/F7DF6PQS. https://www.usgs.gov/centers/eros/science/usgs-eros-archive-digital-elevation-global-30-arc-second-elevation-gtopo30

Gutenberg, R. & Richter, C. F., 1944. Frequency of earthquakes in California. Bulletin of the Seismological Society of America 34, 185–188.

Kamai, R. & Hatzor, Y. H., 2008. Numerical analysis of block stone displacements in ancient masonry structures: a new method to estimate historic ground motions. International Journal for Numerical and Analytical Methods in Geomechanics 32, 1321–1340. https://doi.org/10.1002/nag.671

Kondorskaya, N. V. & Shebalin, N. V., 1982. New Catalog of Strong Earthquakes in the Territory of the Soviet Union from Ancient Times till 1977. Boulder, CO, USA, 608 p.

Kujansuu, R., 1964. Recent faults in Finnish Lapland. Geologi 16, 1–30.

Kukkonen, I. T., Olesen, O., Ask, M. V. S. & the PFDP Working Group, 2010. Postglacial Faults in Fennoscandia: Targets for scientific drilling. GFF 132, 71–81. https://doi.org/10.1080/11035891003692934.

Lagerbäck, R., 1992. Dating of Late Quaternary faulting in northern Sweden. Journal of the Geological Society 149, 285–291. https://doi.org/10.1144/gsjgs.149.2.0285

Lagerbäck, R. & Sundh, M., 2008. Early Holocene faulting and paleoseismicity in northern Sweden. SGU Research Paper C836, 80 p.

Lomtadze, V. D. 1977. Engineering geology. Engineering geodynamics. L: Nedra, 479 p. (In Russian).

Lukashov, A. D., 1995. Paleoseismotectonics in the northern part of lake Onega (Zaonezhsky peninsula, Russian Karelia). Geological Survey of Finland. Nuclear Waste Disposal Research Report Yst-90, 36 p.

Lunina, O. V., Andreev, A. V. & Gladkov, A. S., 2012. The Tsagan earthquake of 1862 on Lake Baikal revisited: a study of secondary coseismic soft-sediment deformation. Russian Geology and Geophysics 53, 571–587. https://doi.org/ 10.1016/j.r gg.2012.04.007.

Marakhanov, A. V. & Romanenko, F. A., 2014. New data on postglacial seismic dislocations of the Northern Karelia (Karelian coast of the White Sea). Yudakhin Readings. Geodynamics and ecology of the Barents region in the XXIst century. Proceedings of the All-Russian Conference with International Participation, Institute of Ecological Problems of the North: Arkhangelsk, Russia, 15–18 September 2014, p.p. 137–140. (In Russian).

McCalpin, J. P., 2009. Paleoseismology. International Geophysics 95. Elsevier, ISSN 0074-6142, 802 p. https://doi.org/10.1016/S0074-6142(09)95001-X

McGarr, A. & Fletcher, J. B., 2007. Near-fault peak ground velocities from earthquake and laboratory data. Bulletin of the Seismological Society of America 97, 1502–1510. https://dx.doi.org/10.1785/0120060268

Michetti, A. M., Esposito, E., Guerrieri, L., Porfido, S., Serva, L., Tatevossian, R., Vittori, E., Audemard, F., Azuma, T., Clague, J., Comerci, V., Gürpinar, A., Mc Calpin, J., Mohammadioun, B., Mörner, N. A., Ota, Y. & Roghozin, E., 2007. Intensity Scale ESI 2007. In: Guerrieri, L. & Vittori, E. (eds.), Mem. Descr. Carta Geologica d'Italia, Servizio Geologico d'Italia, Dipartimento Difesa del Suolo, APAT, Rome, Italy, 74 p.

Mitrofanov, F. P., 2001. Geological Map of the Kola Region 1:1 000 000. Geological Institute of KSC RAS, Apatity.

Mitrofanov, F. P. & Zozulya, D. R., 2002. Major geological sights of the Kola Peninsula. Apatity. 160 p.

Mörner, N.-A., 2004. Active Faults in Fennoscandia, Especially Sweden: Primary Structures and Secondary Effects. Tectonophysics 380, 139–157. https://doi.org/10.1016/j.tecto.2003.09.018

Mörner, N.-A., 2011. Paleoseismology: The Application of Multiple Parameters in Four Case Studies in Sweden. Quaternary International 242, 65–75. https://doi.org/10.1016/j.quaint.2011.03.054

Mushketov, I., & Orlov, A., 1893. Earthquake catalogue of Russian Empire. Zap. RGO, St. Petersburg 26, 582 p. (In Russian).

Niemelä, J., Ekman, I. & Lukashov, A., 1993. Quaternary deposits of Finland and northwestern part of Russian Federation and their resources. Scale 1: 1 000 000. Geological Survey of Finland and Russian Academy of Science, Institute of Geology, Petrozawodsk.

Nikolaeva, S. B., 2001. Paleoseismic manifestations in the north-eastern part of the Baltic Shield and their geological and tectonic position. Geomorphology 4, 66–74. (In Russian).

Nikolaeva, S. B., 2006. Seismogenic Deformations in Early Holocene Sediments of the Pechenga River Terrace (Kola Peninsula). Doklady Earth Sciences 406, 4–7. https://doi.org/10.1134/s1028334x06010028.

Nikolaeva, S. B., 2008. Disastrous earthquakes in the vicinities of the town of Murmansk: Paleoseismological and geological evidence. Journal of Volcanology and Seismology 2, 189–198. https://doi.org/10.1134/S0742046308030068

Nikolaeva, S. B., 2009. Seismites in Late Pleistocene and Holocene deposits of the northwestern Kola region (northern Baltic Shield). Russian Geology and Geophysics 50, 636–642. https://doi.org/10.1016/j.rgg.2008.12.009

Nikolaeva, S. B., 2013. Evidence of seismic events on the coast of Murman in the Late Glacial and Holocene. News of the Russian geographical society 145, 53–65. (In Russian).

Nikolaeva, S. B., Nikonov, A. A., Shvarev, S. V. & Rodkin, M. V., 2018. Detailed paleoseismological research on the flank of the Lake Imandra depression (Kola region): new approaches and results, Russian Geology and Geophysics 59, 697–708. http://dx.doi.org/10.1016/j.rgg.

Nikonov, A. A., 1964. Development of the relief and paleogeography of the Anthropogen in the west of the Kola Peninsula. M: Nauka, 182 p. (In Russian).

Nikonov, A. A. & Zykov, D. S., 1996. Paleoseismodeformations in Eastern Fennoscandia. Seismology in Europe. XXV General Assembly. Sept. 9–10, 1996. Reykjavik, Iceland, p.p. 122–127.

Nikonov, A. A., Shvarev, S. V., Sim, L. A., Rodkin, M. V., Biske, Y. S. & Marinin, A. V., 2014. Paleoseismodeformations of hard rocks in the Karelian isthmus. Doklady Earth Sciences 457, 1008–1013. https://doi.org/10.1134/s1028334x14080145

Obermeier, S. F., Olson, S. M. & Green, R. A., 2005. Field occurrences of liquefaction-induced features: a primer for engineering geologic analysis of paleoseismic shaking. Engineering Geology 76, 209–234. https://doi.org/10.1016/j.enggeo.2004.07.009

Ojala, A. E. K., Markovaara-Koivisto, M., Middleton, M., Ruskeeniemi, T., Mattila, J. & Sutinen, R., 2018. Dating

of seismically-induced paleolandslides in western Finnish Lapland. Earth Surface Processes and Landforms 43, 2449–2462. https://doi.org/10.1002/esp.4408

Ojala, A. E. K., Mattila, J., Ruskeeniemi, T., Palmu, J.-P., Nordbäck, N., Kuva, J. & Sutinen, R., 2019. Postglacial reactivation of the Suasselkä PGF complex in SW Finnish Lapland. International Journal of Earth Sciences, 1049–1065. https://doi.org/10.1007/s00531-019-01695-w

Olesen, O., Blikra, L. H., Braathen, A., Dehls, J. F., Olsen, L., Rise, L., Roberts, D., Riis, F., Faleide, J. I. & Anda, E., 2004. Neotectonic deformation in Norway and its implications: a review. Norwegian Journal of Geology 84, 3–34.

Olesen, O., Bungum, H., Dehls, J., Lindholm, C., Pascal, C. & Roberts, D., 2013. Neotectonics, seismicity and contemporary stressfield in Norway–mechanisms and implications. In: Olsen, L, Fredin, O, Olesen, O. (Eds.), Quaternary Geology of Norway. Geological Survey of Norway, Special Publication 13, 145–174.

Owen, G. & Moretti, M., 2011. Identifying triggers for liquefaction-induced soft-sediment deformation in sands. Sedimentary Geology 235, 141–147. https://doi.org/10.1016/j.sedgeo.2010.10.003

Reimer, P. J., Bard, E., Bayliss, A., Beck, J. W., Blackwell, P. G., Ramsey, C. B., Buck, C. E., Cheng, H., Edwards, R. L., Friedrich, M., Grootes, P. M., Guilderson, T. P., Haflidason, H., Hajdas, I., Hatte, C., Heaton, T. J., Hoffmann, D. L., Hogg, A. G., Hughen, K. A., Kaiser, K. F., Kromer, B., Manning, S. W., Niu, M., Reimer, R. W., Richards, D. A., Scott, E. M., Southon, J. R., Staff, R. A., Turney, C. S. M. & van der Plicht, J. 2013. Intcal13 and Marine13 radiocarbon age calibration curves 0-50,000 years cal BP. Radiocarbon 55, 1869–1887. https://doi.org/10.2458/azu_js_rc.55.16947

Rodkin, M. V. & Korzhenkov, A. M., 2019. Estimation of maximum mass velocity from macroseismic data: A new method and application to archeoseismological data. Geodesy and Geodynamics 10, 321–330. https://doi.org/10.1016/j.geog.2018.06.010

Rodkin, M. V., Nikonov, A. A., & Shvarev, S. V., 2012. Evaluation of quantities of seismic effects on deformations and displacements in rock massifs. Geodynamics and Tectonophysics 3, 203–237. (In Russian). https://doi.org/10.5800/gt-2012-3-3-0072

Seilacher, A., 1969. Fault-graded beds interpreted as seismites. Sedimentology 13, 155–159. https://doi.org/10.1111/j.1365-3091.1969.tb01125.x

Shvarev, S. V. & Rodkin, M. V., 2018. Structural Position and Parameters of the Paleo-earthquakes in the Area of Vottovaara Mountain (Middle Karelia, Eastern Part of the Fennoscandian Shield). Seismic Instruments 54, 199–218. https://doi.org/10.3103/S0747923918020093

Shvarev, S. V., Nikonov, A. A, Rodkin, M. V. & Poleshchuk, A.V., 2018. The active tectonics of the Vuoksi fault zone in the Karelian isthmus: parameters of paleoearthquakes estimated from bedrock and soft-sediment deformation features. Bulletin of the Geological Survey of Finland 90, 257–273. https://doi.org/10.17741/bgsf/90.2.009

Smith, C. A., Sundh, M. & Mikko, H., 2014. Surficial geology indicates early Holocene faulting and seismicity, central Sweden. International Journal of Earth Sciences 103, 1711–1724. https://doi.org/10.1007/s00531-014-1025-6.

Stroeven, A. P., Hättestrand, C., Kleman, J., Heyman, J., Fabel, D., Fredin, O., Goodfellow, B. W., Harbor, J. M., Jansen, J. D., Olsen, L., Caffee, M. W., Fink, D., Lundqvist, J., Rosqvist, G. C., Strömberg, B. & Jansson, K. N., 2016. Deglaciation of Fennoscandia. Quaternary Science Reviews 147, 91–121. http://dx.doi.org/10.1016/j.quascirev.2015.09.016

Subetto, D. A, Shvarev, S. V., Nikonov, A. A., Zaretskaja, N. E., Poleshchuk, A. V. & Potakhin, M. S., 2018. New evidence of the Vuoksi River origin by geodynamic cataclysm. Bulletin of the Geological Survey of Finland 90, 275–289. https://doi.org/10.17741/bgsf/90.2.010

Sutinen, R., Hyvönen, E., Middleton, M. & Airo M-L., 2018. Earthquake-induced deformations on ice-stream landforms in Kuusamo, eastern Finnish Lapland. Global and Planetary Change 160, 46–60. https://doi.org/10.1016/j.gloplacha.2017.11.011.

Verzilin, N. N., Bobkov, A. A., Kulkova, M. A., Nesterov, E. M., Nesterova, L.A. & Madianova, N. V., 2013. On age and formation of modern dissected relief of Kola Peninsula northern part. Vestnik of Saint-Petersburg University 7, 79–93. (In Russian).

Wheeler, R.L., Ettensohn, F.R., Rast, N. & Brett, C.E., 2002. Distinguishing seismic from nonseismic soft-sediment structures: criteria from seismic-hazard analysis. Special papers of Geological society of America, 1–12. https://doi.org/10.1130/0-8137-2359-0.1

Yevzerov, V. Y., 1988. Deglaciation of the Kola Peninsula and the Belomorian depression. Abstract of Second Quaternary Environment of the Eurasian North (QUEEN): workshop. Saint Peterburg, Russia, 5–8 February, 55 p.

Yevzerov, V. Y. & Nikolaeva, S. B., 2007. Geological evidence of the seismisity in the Kola region during the late Pleistocene and Holocene. Geological Survey of Finland. Special Paper 46. Espoo, 129–133.

Zazovskaya, E. P., 2016. Radiocarbon dating – modern state, problem, prospects of development and use in archaeology. Bulletin of archeology, anthropology and ethnography 1, 151–164. https://doi.org/10.20874/2071-0437-2016-32-1-151-164